

Chapter 3

Sensorless PM-Drive Aspects

**Christian Grabner, Johannes Gragger, Hansjoerg Kapeller,
Anton Haumer, and Christian Kral**

Abstract The development procedure of permanent magnet drives for sensor less operation beginning from standstill under overload conditions has to consider different design aspects coevally. First, the robust rotor position sensing by test signal enforces a design with a strongly different behavior of the spatial dq-oriented differential inductance values. Therefore, the interior rotor magnet array arrangement is from principle predestinated for the controlled sensor less mode including standstill. Fortunately, in order to reduce costs, the distinct reluctance torque capability of such interior magnet arrangement is additionally used for a significantly increased torque by applying a pre-oriented stator current space vectors within the quasi-steady control.

Keywords Sensorless vector control · machine design · inductance modeling · nonlinear saturation effects

3.1 Introduction

The overall design process of modern high performance and cost effective permanent magnet drives is still a complex multi physic task, as shown in Fig. 3.1 [1]. In order to achieve both a high efficiency and a simple controllability of the motor, many proposed designs have to be investigated systematically by the ‘virtual design’ approach based on manifold numerical commercial available simulation tools [2]. During the electromagnetic machine, the electrical power converter and the software based control design process a lot of high sophisticated simulations take place in order to verify the desired performance behavior in advance [3, 4].

C. Grabner (✉), J. Gragger, H. Kapeller, A. Haumer, and C. Kral
Electric Drive Technologies, Austrian Institute of Technology,
Giefinggasse 2, 1210 Vienna, Austria
e-mail: christian.grabner@ait.ac.at; johannes.gragger@ait.ac.at; hansjoerg.kapeller@ait.ac.at;
anton.haumer@ait.ac.at; christian.kral@ait.ac.at

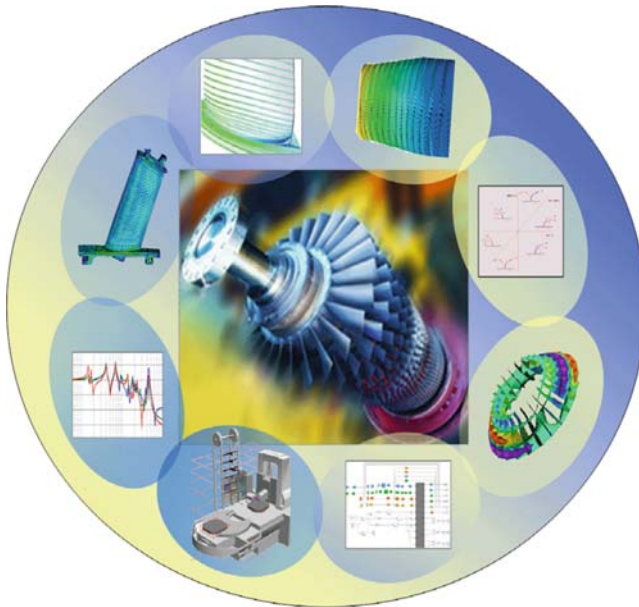


Fig. 3.1 Multi-physical design process of drives



Fig. 3.2 Typical interior permanent magnet machine construction (*left*) and power electronic with DC-link (*right*)

It takes implicit account of important geometric and crucial nonlinear magnetic properties of the machine, as well as the converter topology, which mainly govern the relevant drive performance aspects [5, 6]. Moreover, the inclusion of basic control features within the circuit approach allows the simulation of the complete drive system in advance. A deeper insight into the 4.5 kW permanent magnet machine and the according power converter with the implemented control algorithm is given in Fig. 3.2, where the typical interior permanent magnet structure as well as the

Table 3.1 Machine properties

Rated power	Copper losses	Iron losses	Friction, fan losses	Balance losses
4.5 kW	246 W	103 W	55 W	38 W

Table 3.2 Converter properties

Rated power	Pulses	Output current	Frequency	Efficiency
5 kVA	2 kHz	14 A	0–200 Hz	95%

DC-link capacitors of the power module are obvious. The rated values of machine and converter are partially listed in Tables 3.1 and 3.2.

3.2 Sensorless Control Mode

The vector control mode operates the permanent magnet motor like a current source inverter driven machine applying a continuous current modulation [7]. Therefore, a very precise knowledge of the rotor position is necessary. This could be achieved by processing the response of the machine to arbitrarily injected high frequency test signals, whereby special anisotropic properties of the machines rotor are required. The vector control software itself is adapted to the hardware system depicted in Fig. 3.2.

3.2.1 Nonlinear Motor Model

The practical realization of the control structure is fortunately done within the rotor fixed (d, q) reference system, because the electrical stator quantities can there be seen to be constant within the steady operational state [8]. The stator voltage and flux linkage space vectors are therefore usually formulated in the (d, q) rotor reference frame as

$$\underline{u}_{Sdq}(\tau) = r_S \underline{i}_{Sdq}(\tau) + \frac{d\underline{\psi}_{Sdq}(\tau)}{d\tau} + j\omega \underline{\psi}_{Sdq}(\tau), \quad (3.1)$$

$$\underline{\psi}_{Sdq}(\tau) = \underline{l}_S(\underline{i}_{Sdq}) \underline{i}_{Sdq}(\tau) + \underline{\psi}_{Mdq}, \quad (3.2)$$

whereby r_s denotes the normalized stator resistance. The inductance matrix is written as

$$\underline{l}_S = \begin{pmatrix} l_{Sd}(i_{Sd}) & 0 \\ 0 & l_{Sq}(i_{Sq}) \end{pmatrix}. \quad (3.3)$$

It considers, e.g., only main inductance changes in the spatial d-direction due to the d-current component of the stator current space vector, whereas influences due to the q-current component are neglected in (3.3). With respect to the q-direction, the same aspects are valid in (3.3). Consequently, the relation (3.3) has a symmetrical diagonal shape, whereas cross-coupling effects due to saturation effects are omitted. The inclusion of some basic identities for the magnet flux space vector in the (d, q) system, namely

$$\frac{d\underline{\psi}_{Mdq}}{d\tau} = 0, \quad \underline{\psi}_{Mdq} = \psi_M + j0 \quad (3.4)$$

reduces the system (3.1–3.3) to the simpler set of equations

$$u_{sd}(\tau) = r_S i_{sd}(\tau) + l_{sd,\text{diff}} \frac{d}{d\tau} i_{sd}(\tau) - \omega l_{sq} i_{sq}(\tau), \quad (3.5)$$

$$u_{sq}(\tau) = r_S i_{sq}(\tau) + l_{sq,\text{diff}} \frac{d}{d\tau} i_{sq}(\tau) + \omega l_{sd} i_{sd}(\tau) + \omega \psi_M. \quad (3.6)$$

Thereby, (3.5 and 3.6) distinguishes between main inductance values l_{sd} , l_{sq} , governing the rated operational state, and differential inductances

$$l_{sd,\text{diff}} = l_{sd}(i_{sd}) + i_{sd} \frac{d}{di_{sd}} l_{sd}(i_{sd}), \quad (3.7)$$

$$l_{sq,\text{diff}} = l_{sq}(i_{sq}) + i_{sq} \frac{d}{di_{sq}} l_{sq}(i_{sq}), \quad (3.8)$$

which are mainly influencing the voltage drops due to the (d, q) related time-dependent current changes in (3.5 and 3.6). It is thereby obviously from e.g. (3.7) that there is a direct vice-versa relation between the differential inductance $l_{sd,\text{diff}}$ and the main inductance l_{sd} , if the saturation dependency from the d-current component is well known. Unfortunately, both Eqs. (3.5 and 3.6) are always directly coupled without the exception of standstill. That fact is very unsuitable for the design of the current controller. Thus, with regard to the used vector control topology, a more favorable rewritten form of (3.5 and 3.6) as

$$\begin{aligned} u_d(\tau) &= u_{sd}(\tau) + \omega l_{sq} i_{sq}(\tau) \\ &= r_S i_{sd}(\tau) + l_{sd,\text{diff}} \frac{d}{d\tau} i_{sd}(\tau), \end{aligned} \quad (3.9)$$

$$\begin{aligned} u_q(\tau) &= u_{sq}(\tau) - \omega l_{sd} i_{sd}(\tau) - \omega \psi_M \\ &= r_S i_{sq}(\tau) + l_{sq,\text{diff}} \frac{d}{d\tau} i_{sq}(\tau). \end{aligned} \quad (3.10)$$

with (3.7 and 3.8) is commonly introduced.

3.2.2 Simplified Block Diagram of Closed-Loop Control

The control schema in accordance to (3.9 and 3.10) is realized by using the decoupling network of Fig. 3.3 in Fig. 3.4 with respect to the (d, q) axis notation as a two-step overlaid cascade structure [7, 8].

The decoupling phenomena (3.9 and 3.10) is build up with both fictive voltages u_d , u_q according to Fig. 3.3. So, both (d, q) axes related controller in (3.9 and 3.10) can be adjusted independently from each other. The outer speed cascade allows adjusting a pre-set speed value n_{def} , after getting smoothed by a PT1-element.

The output of the PI speed controller is also smoothed by a PT1-element and restricted by the thermal I^2t -protection in order to avoid thermal damages. The PI speed controller has a moderate sampling rate and determines the demanded q-current component. In a simplified application, the drive is operated with a default zero d-current component in order to achieve maximal torque output. The actual measured electrical phase currents are transformed to the rotor fixed (d, q) reference system and continuously compared to the demanded d- and q-current components at the innermost current cascade structure. With regard to the d- and q-axis separation, the generated PI-current controller output voltages u_d , u_q are almost seen as fictive quantities in Fig. 3.5, from which the de-coupling-circuit given in Fig. 3.6 calculates the real demanded stator voltage components u_{sd} , u_{sq} for the normal operation afterwards.

3.2.3 Injected High Frequency Test Signals

Test signals of very high frequency are superimposed to the demanded stator voltage components u_{sd} , u_{sq} and are further treated within the power stack ASIC in order to generate the according space vectors in Fig. 3.4. Thereby, the desired current test signals i_{test} are almost related in the d-direction of the estimated (d', q') reference

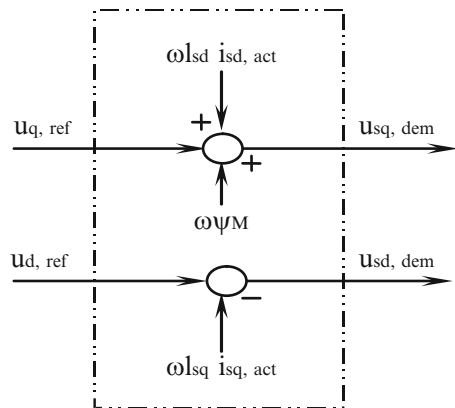


Fig. 3.3 Block diagram of the decoupling-circuit

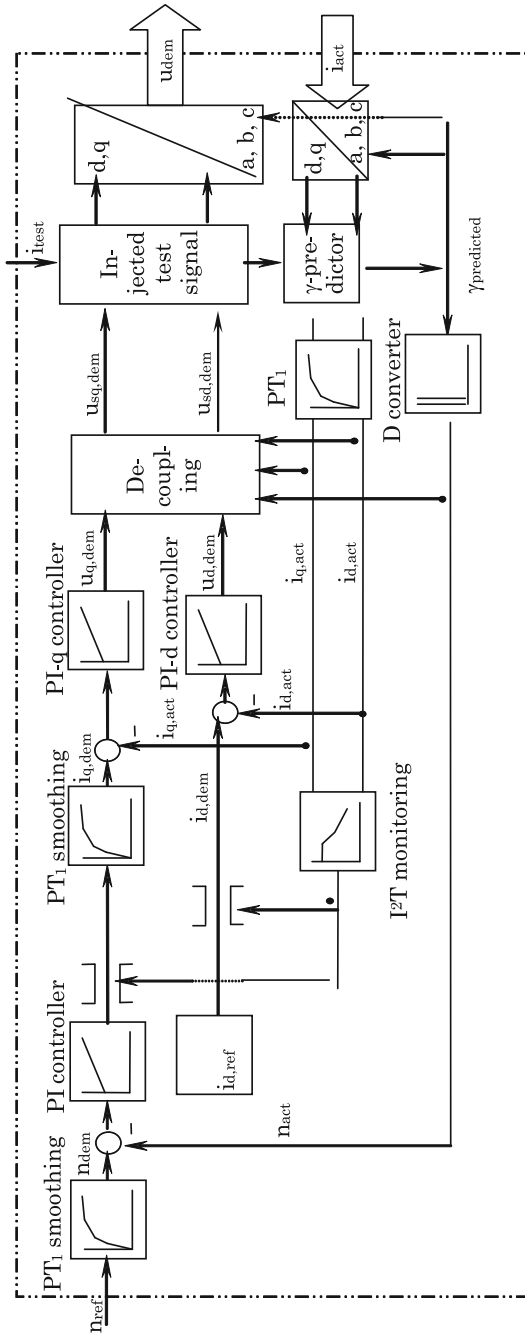


Fig. 3.4 Outline of important devices of the vector controlled permanent magnet motor by neglecting any feed-forward loops

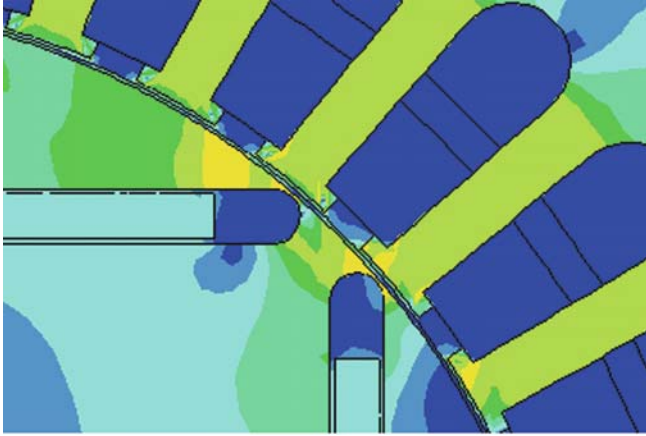
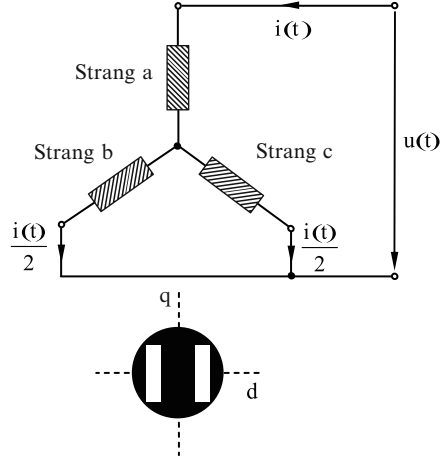


Fig. 3.5 Standstill set-up for the determination of saturable main and differential d-inductances taking account also account of the joke saturation due to the embedded magnets of a electrical two-pole machine

Fig. 3.6 Standstill set-up for the determination of saturable main and differential q-inductances of a electrical two-pole machine



system of the given rotor in Fig. 3.4. Thereby the estimated (d' , q') and the real (d , q) system could differ and hence, the difference is thereby treated by a PLL.

If the measured high frequency content of the q-current component of the PLL is zero, both systems (d' , q') and (d , q) match. So, the position would be correctly estimated. But if there occurs also a d-current component due to the applied test vector in a wrong direction, a difference between (d' , q') and (d , q) would occur. For the correctness of those algorithm it is essential, that the influence of the saturation dependent parameters (3.7 and 3.8) of the machine are laying between safety limiting values.

3.3 Space Dependent Inductances

Inductances are governed by various aspects, whereby the geometric properties and the occurring magnetic saturation of the lamination have a significant impact [9]. Moreover, the magnetic circuit is almost pre-saturated due to the inserted embedded permanent magnets. So, the main task is to set-up a straightforward numerical procedure for the evaluation of those equivalent circuit characteristics with the transient Finite Element approach. Thus, the inductances (3.7 and 3.8) are derived indirectly from (d, q) space dependent flux-current characteristic.

The proposed origin design of flux barriers between the magnets shown in Fig. 3.7 influences the previous parameters (3.7 and 3.8) as well as the torque output and therefore also the drive performance. The desired ratio between both inductances (3.7 and 3.8) can be obtained by the choice of the air gap length, the degree of coverage of the permanent magnets based on the pole pitch of the machine, and the flux barriers between the poles [10, 11]. With respect to mechanical aspects circular ends are always favorable in Fig. 3.7. An optimum distance between the rotor surface and the hole of the magnets has to stand with the mechanical strength and the magnetic saturation. The sheet thickness of the laminated is the smallest possible distance. A smaller distance results in problems with the punching process of the lamina [12].

3.3.1 Set-Up for the Saturation Dependent Differential Inductances Evaluation

The saturation dependent values of (3.7) have to be evaluated in advance with respect to the spatial directions in order to verify the robustness of the drive. In particular

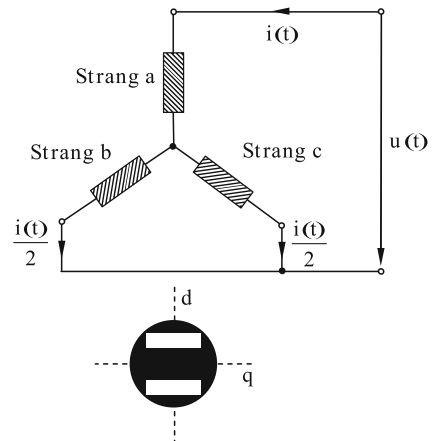


Fig. 3.7 Detail of the rotor design concerning stray fields

the sensor less mode at standstill even at very high currents, which are e.g. necessary for a high pull-out torque have thereby to be covered. If the known q-axis of the rotor is aligned with the q-axis of the stator current space vector, no effect due to the permanent magnet flux (3.4) in the q-axis has to be considered under those assumptions (3.3). The relations (3.7) are therefore valid. The pre-saturation of the lamination due to the magnets is indirectly considered. Neglecting slotting effects, the necessary flux-current characteristic in the q-axis in (3.2), the proposed machine design is treated within the numerical simulation by Finite Elements as a single phase test set-up as shown in Fig. 3.6. If the system is simply fed by a sinusoidal time-dependent voltage, the obtained time-dependent current consumption is mainly non-sinusoidal due to the iron saturation. But the courses are symmetrical to the abscissa.

Contrarily, if the d-axis of rotor coincides with the d-axis of the stator current space vector in Fig. 3.5, the numerical calculated time dependency of the d-current inside the machine represents a non-sinusoidal course with a constant offset, caused by the magnetized magnets within the lamination.

3.3.2 Saturation Dependent Differential and Main Synchronous Inductances

With the aid of commercial numerical field calculation tools, the obtained flux-current relation (3.3) and consequently the differential and the main inductance (3.7) courses are straightforward derived with respect to the (d, q) notation as shown in Figs. 3.8 and 3.9. Thereby, saturation within higher current magnitudes enforces that both d- and q-characteristics become very similar, which means, that the test signals response is equal in each direction and no distinction could be achievable. The dependency of the main inductance shown in Fig. 3.9 shows along the complete current range a distinct difference. Thereby, both relations (3.7 and 3.8) could

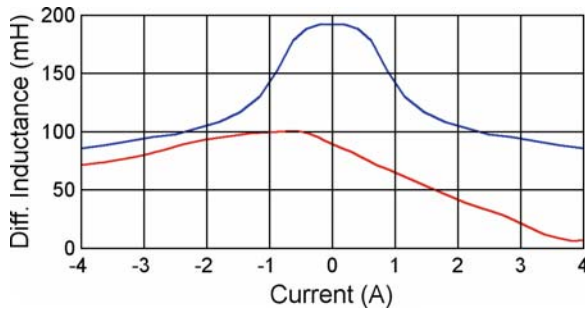


Fig. 3.8 Dependency of d-axis differential inductance from d-current (*red*) and q-axis differential inductance from q-current (*blue*)

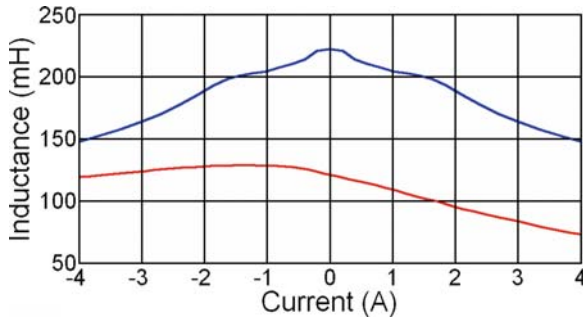


Fig. 3.9 Dependency of d-axis main inductance from d-current (*red*) and q-axis differential inductance from q-current (*blue*)

be clearly verified. The previous desired reluctance effects due to different d- and q-inductance values over the complete current magnitude in Fig. 3.9 are fortunately usable even for full- or overload capabilities.

3.4 Conclusion

The design of permanent magnet drives for sensor less operation has to consider different aspects. First, the robust sensing capability of test signals enforces different differential inductances with respect to the (d, q) notation. The influence of occurring saturation to that behavior has to be restricted. In order to improve the torque output due to the usage of the reluctance torque, the anisotropic inductance properties should be significantly different. Thus, a negative d-axis current increases thereby the effective torque of the motor up to e.g. 15%. Moreover, several secondary effect, such as cogging torque, torque ripple, non-sinusoidal shape of no-load voltage and losses, which are worsening the performance of such innovative drives, must be restricted to limiting values. Thus, a coupled transient electromagnetic-mechanical finite element calculation method with directly coupled external circuits is useful, in the case of the voltage waveform, torque ripple and additional losses. The influence of higher harmonics on the design steps becomes visible by this method.

References

1. Nowotny, W., Lipo, T.A.: Vector Control and Dynamics of AC Drives. Clarendon, Oxford (2000)
2. Hendershot, J.R., Miller, T.J.E.: Design of Brushless Permanent Magnet Motors. Oxford University Press, Oxford (1994)

3. Bush, K.G.: *Regelbare Elektroantriebe: Antriebsmethoden, Betriebssicherheit, Instandhaltung*. Verlag Pflaum, München (1998)
4. Salon, J.S.: *Finite Element Analysis of Electrical Machines*. Cambridge University Press, Cambridge (1996)
5. Davat, B., Ren, Z., Lajoic-Mazenc, M.: The movement in field modeling. *IEEE Trans. Magn.* 21(6) (1985)
6. Kohnke, P.: *Theory Reference Released Version 6.1*. Ansys Inc., Canonsburg, PA (April 2002)
7. Vas, P.: *Electrical Machines and Drives: A Space-Vector Theory Approach*. Clarendon, Oxford (1996)
8. Vas, P.: *Vector Control of AC Machines*. Oxford University Press, Oxford (1990)
9. Vas, P.: *Parameter Estimation, Condition Monitoring, and Diagnosis of Electrical Machines*. Clarendon, Oxford (1993)
10. Domack, S.: *Auslegung und Optimierung von permanent- erregten Synchronmaschinen mittels Steuerverfahren und der Methode der finiten Elemente*. Aachen, Verlag Shaker (1994)
11. Kiyomarsi, A., Moallem, M.: Optimal shape design of interior permanent-magnet synchronous motor. *IEEE Conference on electric machines and drives*, pp. 642–648 (2005)
12. Bödefeld, T.H., Sequenz, H.: *Elektrische Maschinen, Eine Einführung in die Grundlagen*. Wien, Springer-Verlag, New York, pp. 230–236 (1971)